Supporting Information for

# Nanoparticle-Decorated Ultrathin $La_2O_3$ Nanosheets as An Efficient Electrocatalysis for Oxygen Evolution Reactions

Guangyuan Yan[1, 2], Yizhan Wang[1], Ziyi Zhang[1], Yutao Dong[1], Jingyu Wang[1], Corey Carlos[1], Pu Zhang[3], Zhiqiang Cao[2, *], Yanchao Mao[3, *], Xudong Wang[1, *]

[1]Department of Material Sciences and Engineering, University of Wisconsin-Madison, Madison, WI 53706, USA

[2]Key Laboratory of Solidification Control and Digital Preparation Technology (Liaoning Province), School of Materials Science and Engineering, Dalian University of Technology, Dalian 116024, People's Republic of China

[3]MOE Key Laboratory of Materials Physics, School of Physics, Zhengzhou University, Zhengzhou 450001, People's Republic of China

*Corresponding authors. E-mail: xudong.wang@wisc.edu (Xudong Wang); caozq@dlut.edu.cn (Zhiqiang Cao); ymao@zzu.edu.cn (Yanchao Mao)

## Supplementary Figures

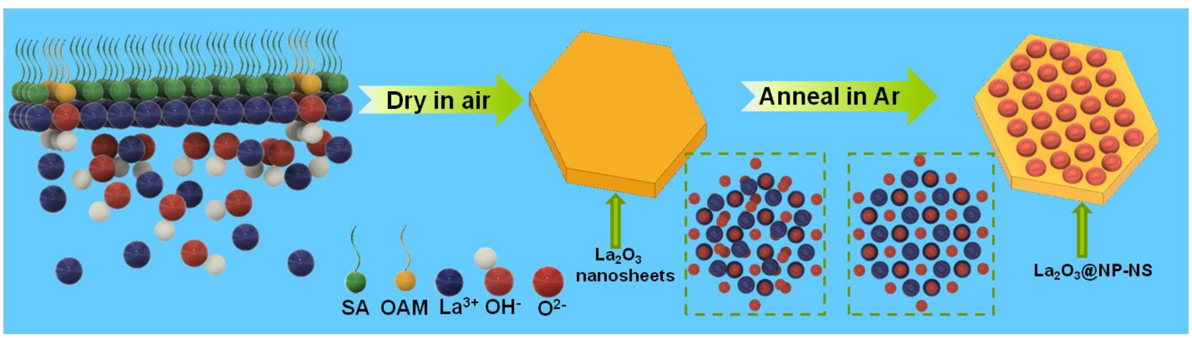


**Fig. S1** Schematic of synthesis process of $La_2O_3$@NP-NS

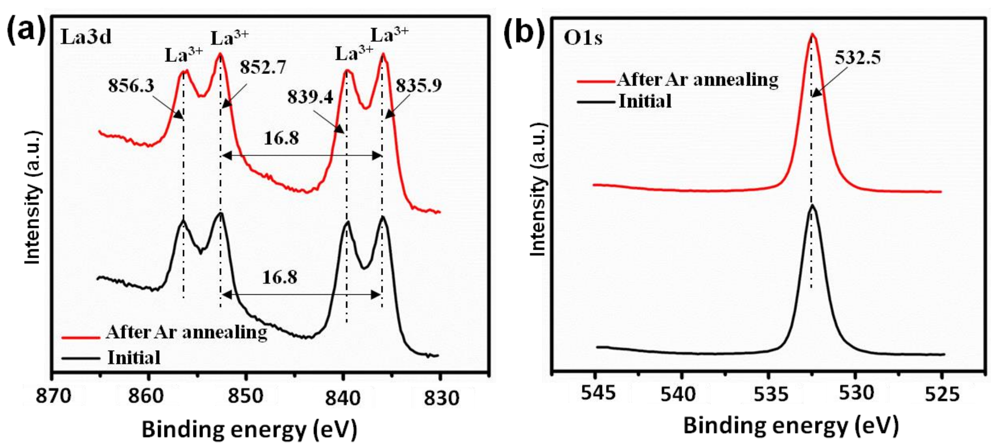


**Fig. S2 a** La 3d and **b** O 1s XPS spectrum of 2.27 nm $La_2O_3$@NP-NS before and after Ar annealing

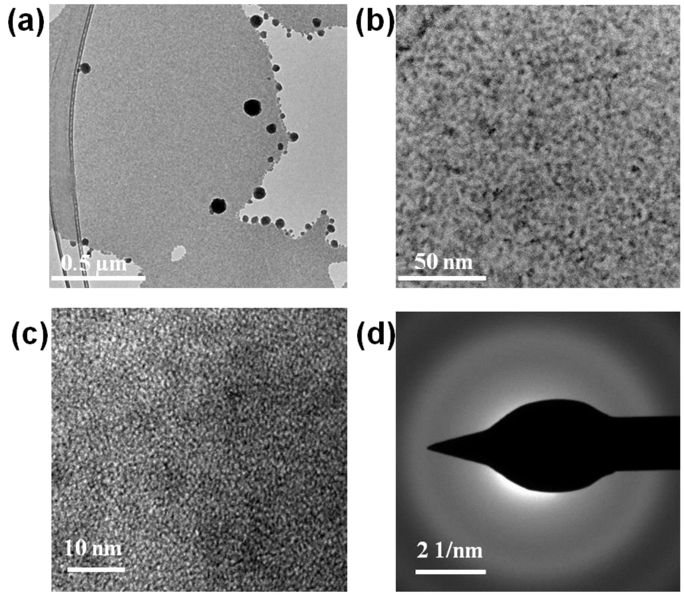


**Fig. S3** Structural characterization of $La_2O_3$ nanosheets before annealing. **a** TEM image of hexagonal $La_2O_3$ nanosheets. **b-c** HRTEM images of $La_2O_3$ nanosheets. **d** Corresponding SAED pattern of $La_2O_3$ nanosheet

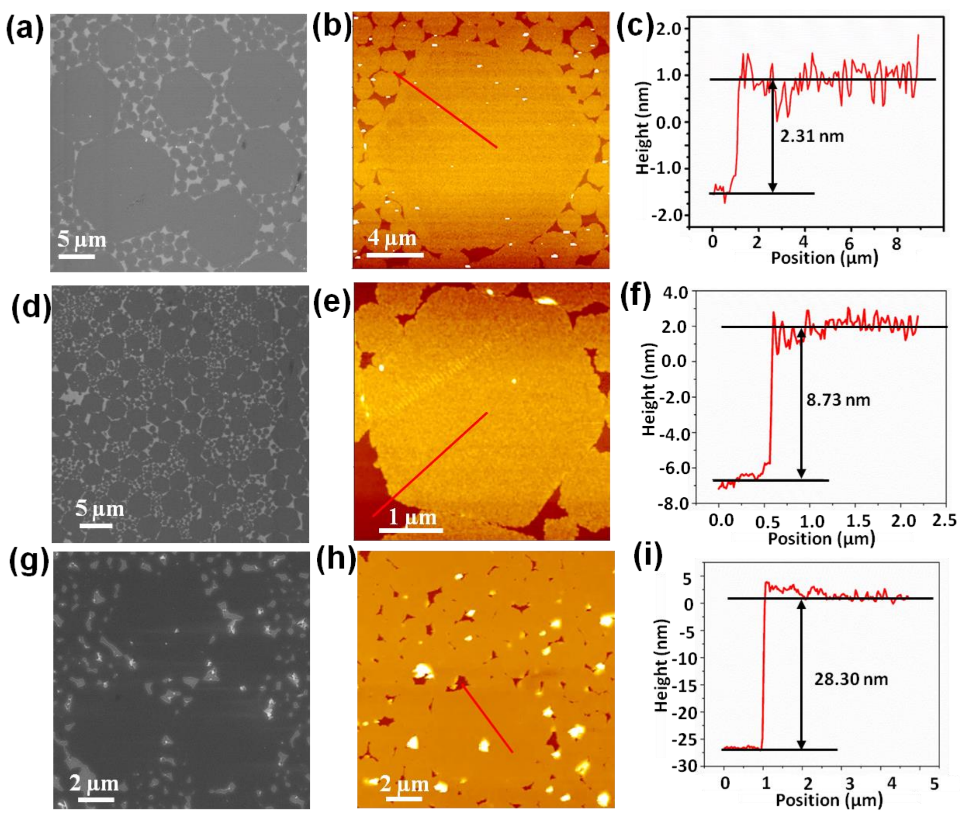


**Fig. S4** $La_2O_3$ nanosheets grown for 5 h at **a-c** 45 °C, **d-f** 60 °C, **g-i** before annealing: **a**, **d**, **g** SEM images, **b**, **e**, **h** AFM topography images, and **c**, **f**, **i** height profiles along the red dashed lines in corresponding AFM topography images

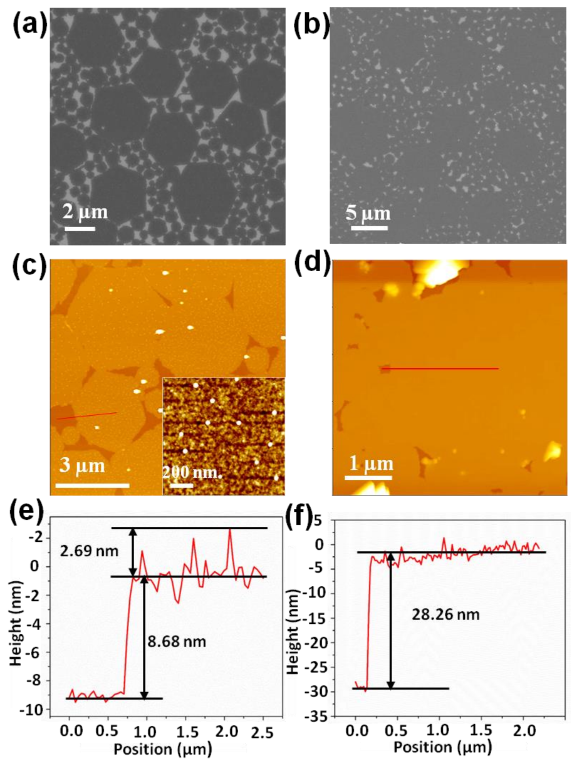


**Fig. S5** Morphology and thickness of 8.68-nm $La_2O_3$@NP-NS and 28.26-nm $La_2O_3$ nanosheets after Ar annealing. **a**–**b** SEM images, **c**–**d** AFM topography images, inset in **c** is high-magnification AFM topography scan of nanosheets, and **e**–**f** height profiles along the red dashed lines in corresponding AFM topography images of nanosheets grown for 5 hours at **a**, **c**, **e** 60 ℃, **b**, **d**, **f** 80 ℃

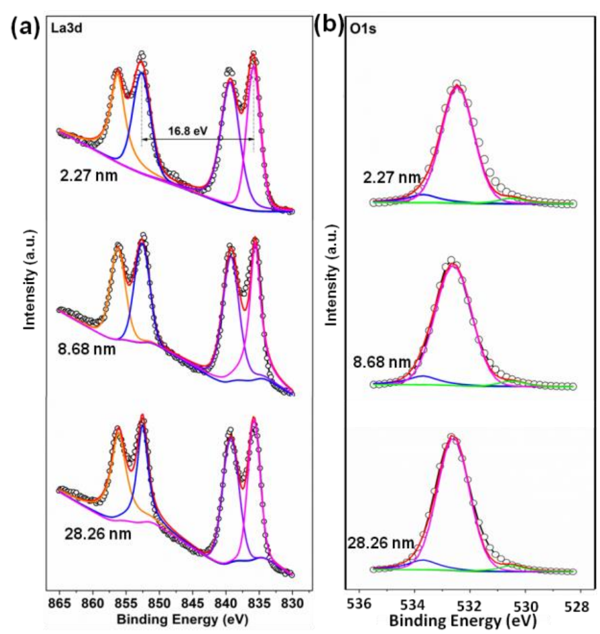


**Fig. S6** Fitted XPS spectrum of characteristic X-ray peak of La 3d **a** and O1s **b** from 2.27-nm $La_2O_3$@NP-NS, 8.68-nm $La_2O_3$@NP-NS, and 28.26-nm thick $La_2O_3$ nanosheets

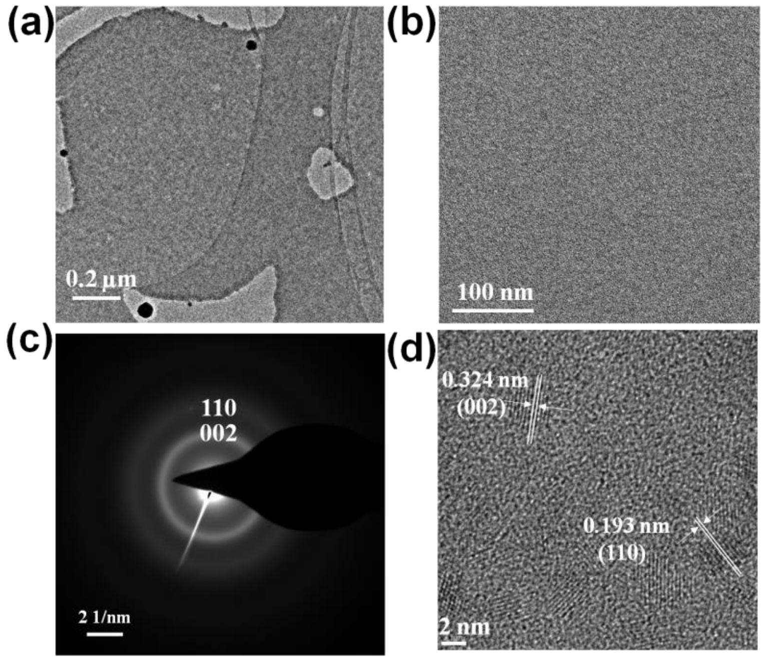


**Fig. S7** Structural characterization of 28.26-nm $La_2O_3$. **a** Low-magnification TEM image of hexagonal $La_2O_3$ nanosheet on a holey carbon TEM grid. **b** High-magnification TEM image. **c** SAED pattern. **d** HRTEM image

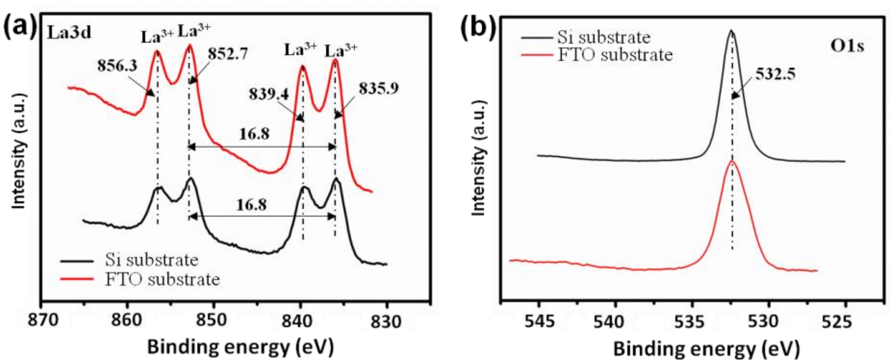


**Fig. S8 a** La 3d and **b** O 1s XPS spectrum of 2.27-nm $La_2O_3$@NP-NS on FTO and Si substrate

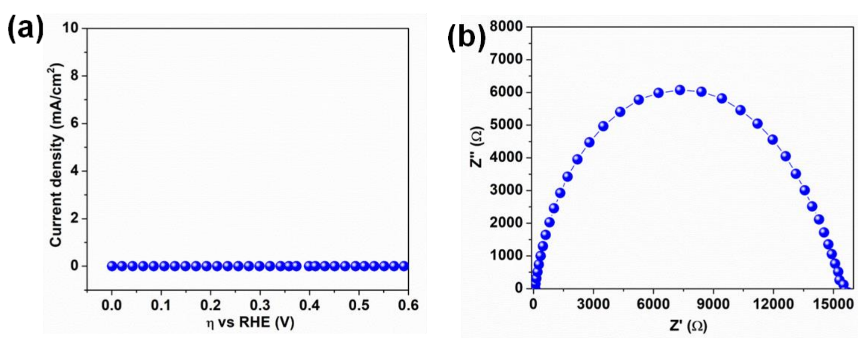


**Fig. S9 a** OER polarization curves of FTO substrate measured in 1 M NaOH aqueous. **b** Nyquist plots of FTO substrate measured in 1 M NaOH solution at a potential of 310 mV vs. RHE

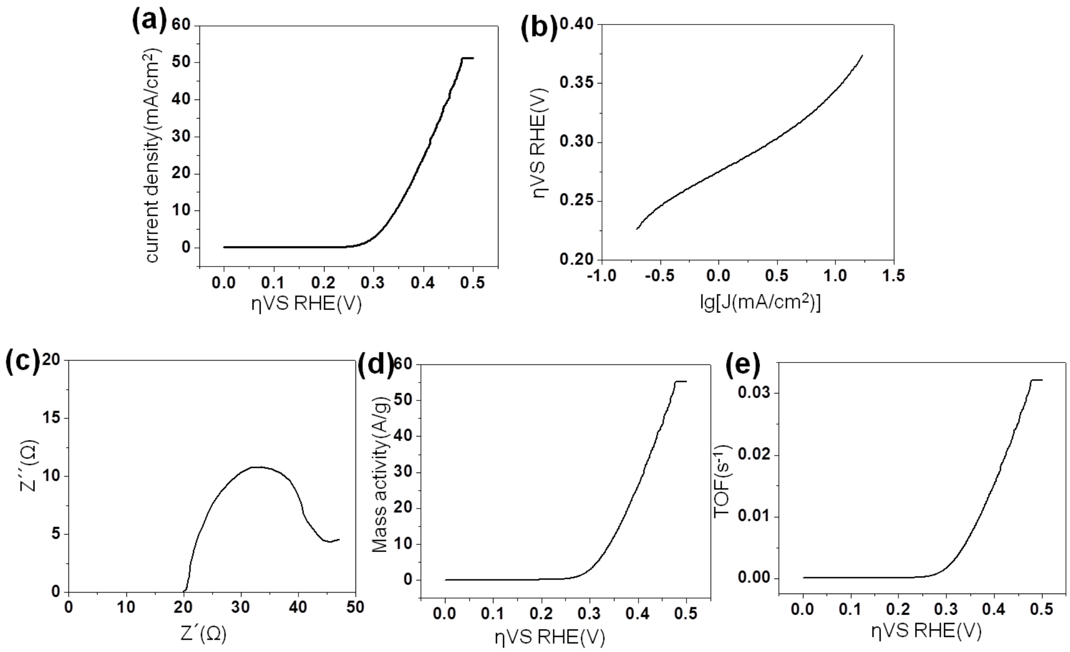


**Fig. S10** Electrocatalytic OER performance of commercial $IrO_2$ powder. **a** OER polarization curves measured in 1 M NaOH solution. **b** Tafel plots. **c** Nyquist plots measured in 1 M NaOH solution at a potential of 310 mV vs. RHE. **d** Mass activity determined from current density as a function of ŋ. **e** TOF determined from j as a function of η

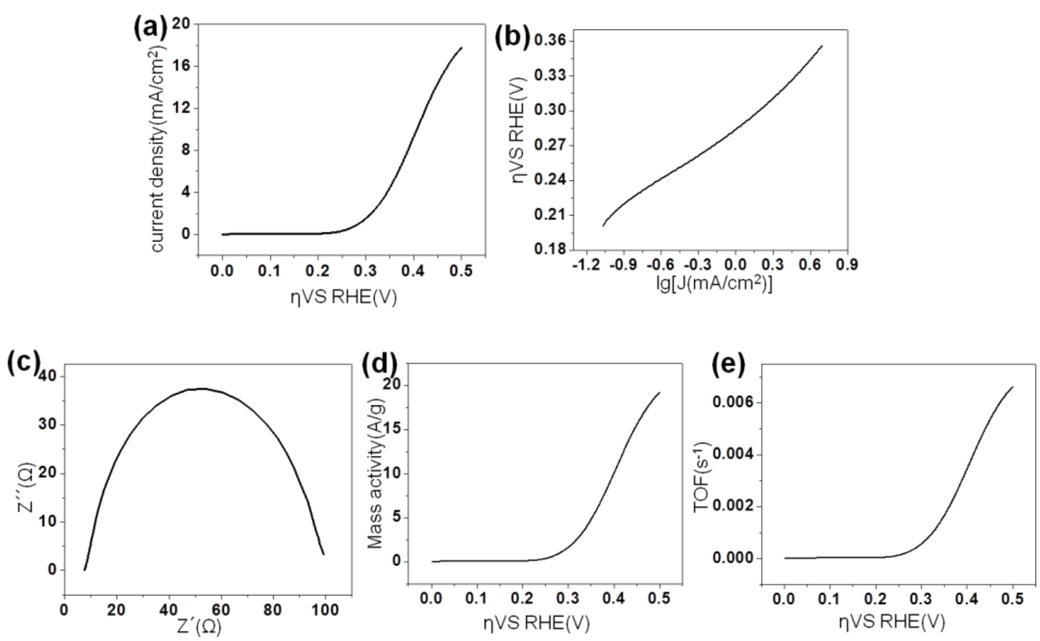


**Fig. S11** Electrocatalytic OER performance of commercial $RuO_2$ powder. **a** OER polarization curves measured in 1 M NaOH solution. **b** Tafel plots. **c** Nyquist plots measured in 1 M NaOH solution at a potential of 310 mV vs. RHE. **d** Mass activity determined from current density as a function of ŋ. **e** TOF determined from j as a function of η

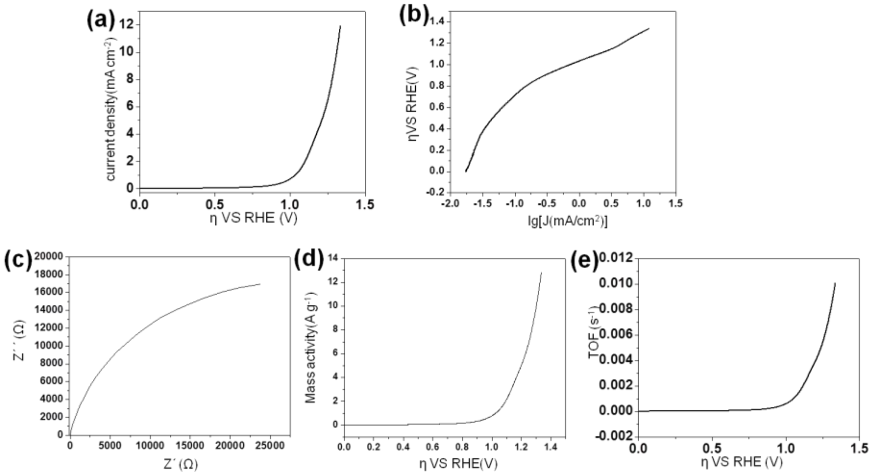


**Fig. S12 a** OER polarization curves measured in 1 M NaOH solution. **b** Tafel plots. **c** Nyquist plots measured in 1 M NaOH solution at a potential of 310 mV vs. RHE. **d** Mass activity determined from current density as a function of ŋ. **e** TOF determined from j as a function of η

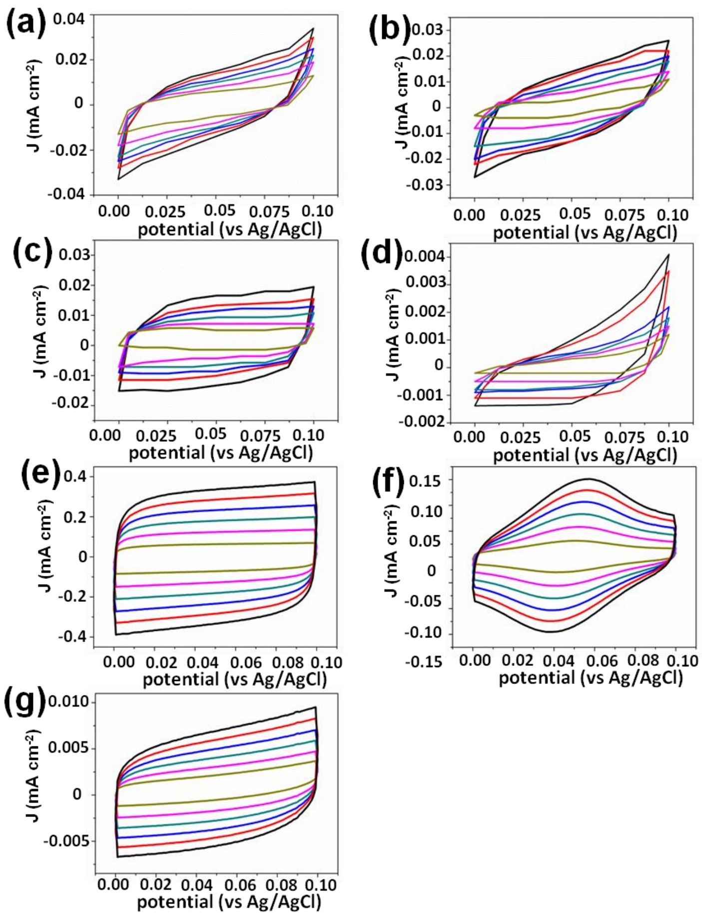


**Fig. S13** Cyclic voltammograms curves of of **a** 2.27-nm $La_2O_3$@NP-NS, **b** 8.68-nm $La_2O_3$@NP-NS and **c** 28.26 nm thick $La_2O_3$ nanosheets, **d** ILE synthesized $La_2O_3$ NPs, commercial **e** $IrO_2$, **f** $RuO_2$, and **g** $La_2O_3$ powder. The scan rates were varied from 10 to 60 mV $s^{-1}$

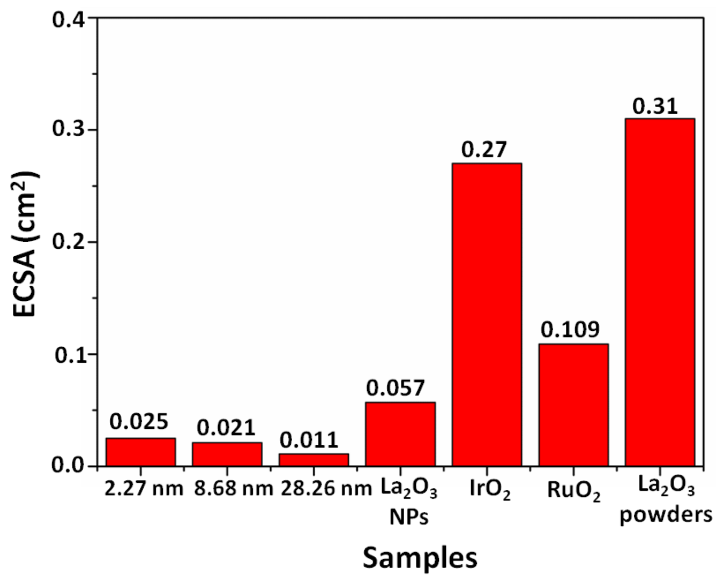


**Fig. S14** ECSA of of **a** 2.27-nm $La_2O_3$@NP-NS, **b** 8.68-nm $La_2O_3$@NP-NS, and **c** 28.26-nm $La_2O_3$ nanosheets, **d** ILE synthesized $La_2O_3$ NPs, commercial **e** $IrO_2$, **f** $RuO_2$, and **g** $La_2O_3$ powder

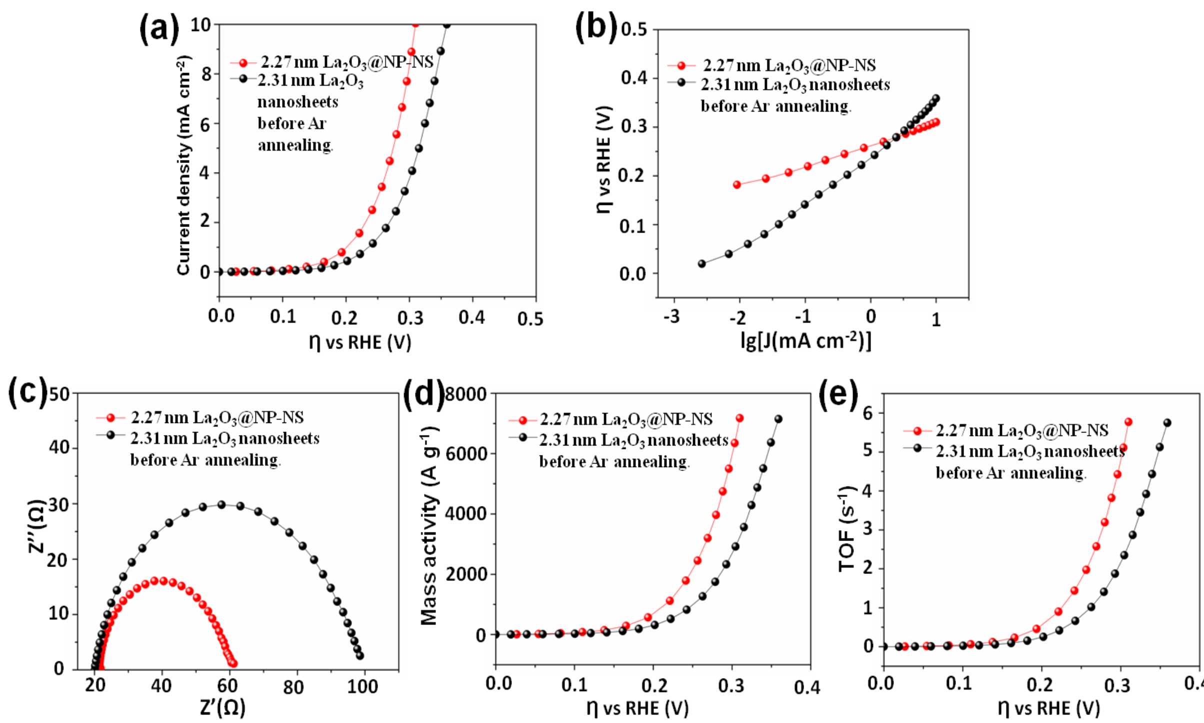


**Fig. S15** Electrocatalytic OER performance comparison of 2.27 nm $La_2O_3$@NP-NS and $La_2O_3$ nanosheets before Ar annealing. a) OER polarization curves measured in 1 M NaOH solution. b) Tafel plots. c) Nyquist plots measured in 1 M NaOH solution at a potential of 310 mV vs. RHE. d) Mass activity determined from current density as a function of η. e) TOF determined from j as a function of η

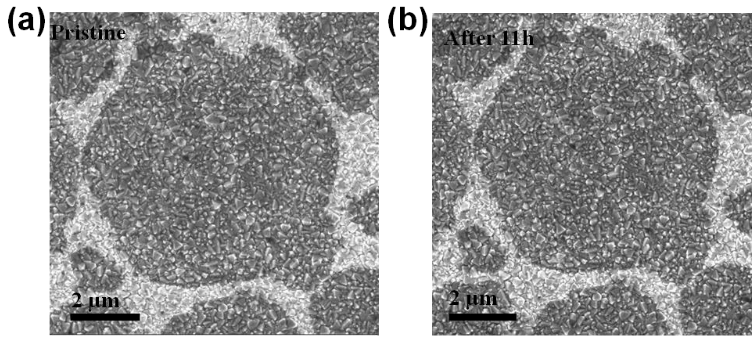


**Fig. S16** SEM images of 2.27 nm $La_2O_3$@NP-NS on FTO substrate before **a** and after **b**11-hour OER

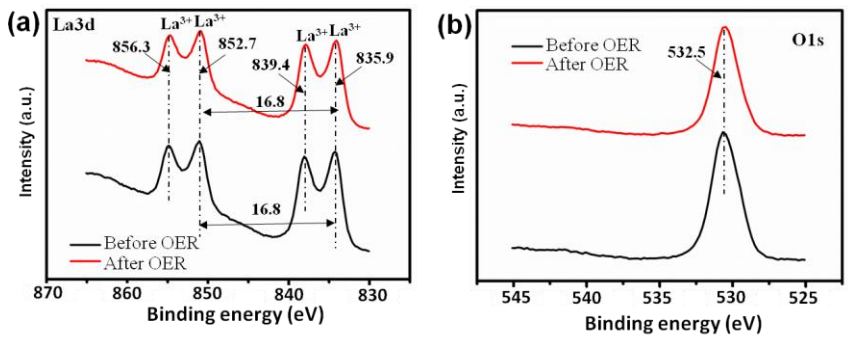


**Fig. S17 a** La 3d and **b** O 1s XPS spectrum of 2.27 nm $La_2O_3$@NP-NS on FTO substrate before and after OER measurement

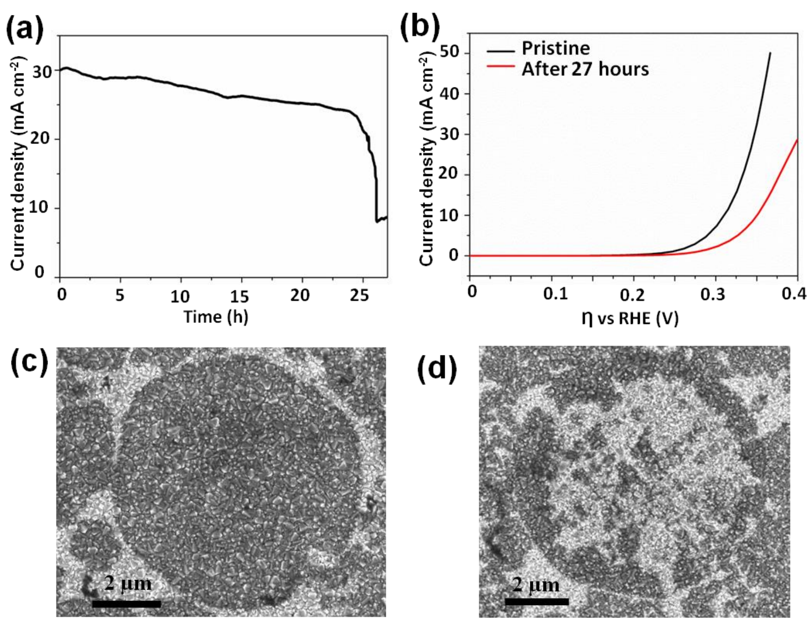


**Fig. S18 a** Current density measured at $\eta = 345$ mV (vs. RHE) as a function of time. **b** OER polarization curves of 2.27-nm $La_2O_3$@NP-NS before and after 27-hour OER. SEM images of 2.27-nm $La_2O_3$@NP-NS on FTO substrate before (**c**) and after (**d**) 27-hour OER

**Table S1** OER performance comparison between this work and other catalysts

| Catalysts | Over potential (mV) @10 mA $cm^{-2}$ | Mass loading (mg $cm^{-2}$) | Mass activity (A $g^{-1}$) @310 mV | TOF ($s^{-1}$) @310 mV | Refs. |
|---|---|---|---|---|---|
| 2.27-nm $La_2O_3$@NP-NS | 310 | 0.0014 | 6666.7 | 5.79 | This work |
| CoFe-LDHs | 310 | 0.2 | 5.0 | - | [S1] |
| NiFe MOFs | 300 | - | < 3100 | - | [S2] |
| $Co_2(OH)_3Cl$ | 270 | 0.105 | 286.4 | 0.73 | [S3] |
| $Co_3O_4/CeO_2$ | 270 | - | - | < 0.25 | [S4] |
| $Co_3O_4$ | 376 | - | - | < 0.39 | [S5] |
| NiFeCr | 342 | - | - | - | [S6] |
| CoFe LDHs | 324 | 0.02 | - | - | [S7] |
| NiO nanoparticle | 335 | 0.02 | 72.5 | 0.0018 | [S8] |
| $Ni_{0.81}Fe_{0.19}O$ | 310 | - | - | <0.26 | [S9] |
| $Co_3O_4$ | 339 | 1.5 | 3.33 | - | [S10] |
| Ni@NC | 390 | 0.4 | 2.5 | 0.136 | [S11] |
| $Co_3O_4$ NW/CC | 320 | 0.82 | 9.76 | - | [S12] |
| $Ni_2P$ nanoparticles | 290 | 0.14 | 142.9 | - | [S13] |
| nNiFe LDH/NGF | 337 | 0.25 | - | - | [S14] |
| $IrO_2$ | 338 | 0.21 | 12.4 | 0.022 | [S15] |
| Mn Oxide | 540 | 0.028 | 71.4 | - | [S16] |

## Supplementary References

[S1] P. Li, M.Y. Wang, X.X. Duan, L.R. Zheng, X.P. Cheng et al., Boosting oxygen evolution of single-atomic ruthenium through electronic coupling with cobalt-iron layered double hydroxides. Nat. Commun. **10**, 1711 (2010). https://doi.org/10.1038/s41467-019-09666-0

[S2] W.R. Cheng, X. Zhao, H. Su, F. Tang, W. Che et al., Lattice-strained metal-organic-framework arrays for bifunctional oxygen electrocatalysis. Nat. Energy **4**, 115-112 (2019). https://doi.org/10.1038/s41560-018-0308-8

[S3] H.L. Jiang, Q. He, X.Y. Li, X.Z. Su, Y.K. Zhang et al., Tracking structural self-reconstruction and identifying true active sites toward cobalt oxychloride precatalyst of oxygen evolution reaction. Adv. Mater. **31**, 1805127 (2019). https://doi.org/10.1002/adma.201805127

[S4] Y. Liu, C. Ma, Q. H. Zhang, W. Wang, P. F. Pan et al., 2D electron gas and oxygen vacancy induced high oxygen evolution performances for advanced $Co_3O_4/CeO_2$ nanohybrids. Adv. Mater. **31**, 1900062 (2019). https://doi.org/10.1002/adma.201900062

[S5] R. R. Zhang, Y. C. Zhang, L. Pan, G. Q. Shen, N. Mahmood et al., Engineering cobalt defects in cobalt oxide for highly efficient electrocatalytic oxygen evolution. ACS Catal. **8**, 3803-3811 (2018). https://doi.org/10.1021/acscatal.8b01046

[S6] Y. Yang, L. Dang, M.J. Shearer, H.Y. Sheng, W.J. Li, et al., Highly active trimetallic nifecr layered double hydroxide electrocatalysts for oxygen evolution reaction. Adv. Energy Mater. **8**, 1703189 (2018). https://doi.org/10.1002/aenm.201703189

[S7] Y.Y. Wang, C. Xie, Z.Y. Zhang, D.D. Liu, R. Chen et al., In situ exfoliated, n-doped, and edge-rich ultrathin layered double hydroxides nanosheets for oxygen evolution reaction.

Adv. Funct. Mater. **28**, 1703363 (2018). https://doi.org/10.1002/adfm.201703363

[S8] K. Fominykh, G.C. Tok, P. Zeller, H. Hajiyani, T. Miller et al., Rock salt Ni/Co oxides with unusual nanoscale-stabilized composition as water splitting electrocatalysts. Adv. Funct. Mater. **27**, 1605121 (2017). https://doi.org/10.1002/adfm.201605121

[S9] A.C. Pebley, E. Decolvenaere, T.M. Pollocka, M.J. Gordon, Oxygen evolution on fe-doped nio electrocatalysts deposited via microplasma. Nanoscale **9**, 15070 (2017). https://doi.org/10.1039/C7NR04302C

[S10] Y. Zhang, B. Ouyang, J. Xu, G. Jia, S. Chen et al., Rapid synthesis of cobalt nitride nanowires: highly efficient and low-cost catalysts for oxygen evolution. Angew. Chem. Int. Ed. **55**, 8670-8674 (2016). https://doi.org/10.1002/anie.201604372

[S11] J. Ren, M. Antonietti, T. P. Fellinger, Efficient water splitting using a simple Ni/N/C paper electrocatalyst. Adv. Energy Mater. **5**, 1401660 (2015). https://doi.org/10.1002/aenm.201401660

[S12] P. Chen, K. Xu, Z. Fang, Y. Tong, J. Wu et al., Metallic $Co_4N$ porous nanowire arrays activated by surface oxidation as electrocatalysts for the oxygen evolution reaction. Angew. Chem. Int. Ed. **54**, 14710-14714 (2015). https://doi.org/10.1002/anie.201506480

[S13] L.A. Stern, L. Feng, F. Song, X. Hu, $Ni_2P$ as a Janus catalyst for water splitting: the oxygen evolution activity of $Ni_2P$ nanoparticles. Energy Environ. Sci. **8**, 2347-2351 (2015). https://doi.org/10.1039/C5EE01155H

[S14] C. Tang, H.S. Wang, H.F. Wang, Q. Zhang, G.L. Tian et al., Spatially confined hybridization of nanometer-sized NiFe hydroxides into nitrogen-doped graphene frameworks leading to superior oxygen evolution reactivity. Adv. Mater. **27**, 4516-4522 (2015). https://doi.org/10.1002/adma.201501901

[S15] F. Song, X. Hu, Exfoliation of layered double hydroxides for enhanced oxygen evolution catalysis. Nat. Commun. **5**, 4477 (2014).https://doi.org/10.1038/ncomms5477

[S16] Y. Li, P. Hasin, Y. Wu, $NixCo_{3-x}O_4$ Nanowire arrays for electrocatalytic oxygen evolution. Adv. Mater. **22**, 1926-1929 (2010). https://doi.org/10.1002/adma.200903896